Anomalous x-ray scattering studies of functional disordered materials

S Kohara[1], H Tajiri[1], C H Song[1], K Ohara[1], L Temleitner[1,2], K Sugimito[1],

A Fujiwara[1], L Pusztai[2], T Usuki[3], S Hosokawa[4], Y Benino[5], N Kitamura[6]

 and K Fukumi[6]

[1] JASRI/ SPring-8, 1-1-1 Kouto, Sayo-cho, Sayo-gun, Hyogo 679-5198, Japan
[2] Wigner Research Centre for Physics, Hungarian Academy of Sciences, H-1525 Budapest, P. O. Box 49, Hungary
[3] Department of Material and Biological Chemistry, Faculty of Science, Yamagata University, 1-4-12 Koshirakawa, Yamagata 990-8560, Japan
[4] Department of Physics, Graduate School of Science and Technology, Kumamoto University, 2-39-1 Kurokami, Kumamoto, 860-8555, Japan
[5] Faculty of Environmental Science and Technology, Okayama University, 1-1-1 Tsushima-naka, Kita-ku, Okayama, 700-8530, Japan
[6] Reserch Institute for Ubiquitous Energy Devices, National Institute of Advanced Industrial Science and Technology, 1-8-31 Midorigaoka, Ikeda, Osaka 563-8577, Japan

E-mail: kohara@spring8.or.jp

Abstract. We have developed anomalous x-ray scattering (AXS) spectrometers, that employ intrinsic Ge detectors and crystal analyzers, at SPring-8. The use of LiF analyzer crystal provides us with an energy resolution of ~ 12 eV. Furthermore, it has been established that the use of AXS technique is essential to reveal the relationship between the atomic structure and its function of a fast phase-change material, $Ge_2Sb_2Te_5$. We were able to address the issue of why the amorphous phase of fast phase change materials is stable at room temperature for a long time despite the fact that it can rapidly transform to the crystalline phase by using a combination of AXS and large scale density functional theory-based molecular dynamics simulations.

1. Introduction

Scattering experiments provide a powerful probe of the structure of disordered materials. X-ray and neutron diffraction have widely been used to make direct measurements of coordination numbers and bond lengths: Fourier transforming the total structure factor, $S(Q)$, yields the pair distribution function, $g(r)$, ($Q=4\pi\sin\theta/\lambda$, 2θ: scattering angle, λ: wavelength of photons or neutrons) a function in real space, by the following equation:

$$g(r) = 1 + \frac{1}{2\pi^2\rho r} \int_{Q\min}^{Q\max} Q[S(Q)-1]\sin(Qr)\,dQ, \qquad (1)$$

where ρ is the atomic number density. In order to obtain detailed structural information from scattering experiments, it is necessary to measure $S(Q)$ up to high Q, since the resolution in real space is determined by Q_{max}. In the case of neutron diffraction, spallation sources make it possible to obtain high Q data with the time of flight technique, so that pulsed neutron diffraction is a powerful tool for

---

[1] To whom any correspondence should be addressed.

structural studies of disordered materials. On the other hand, with the advent of third generation synchrotron sources, it has become possible to perform precise x-ray diffraction experiments on disordered materials, taking accurate diffraction data up to high Q by the use of high intensity photons of high-energy ($E > 50$keV) [1]. Furthermore, a combination of x-ray and neutron diffraction opens up the way to study the structure of disordered materials at atomic to nanoscale [2,3].

Since the development of novel functional disordered materials, such as fast phase-change materials and bulk metallic glasses, has become very important, it is of particular interest to understand the relationship between the atomic/electronic structure and the function of materials. To study complicated functional disordered materials by diffraction/scattering techniques, atom specific probe is necessary. Although x-ray absorption fine structure (XAFS) has widely been used to probe local environment of disordered materials, atom sensitive structure information beyond nearest-neighbor correlations would be desirable for understanding the origin of 'order within disorder' [4], hidden in disordered materials.

The anomalous x-ray scattering (AXS) technique [5,6] is a powerful tool to probe atom sensitive structure in disordered materials. Although the technique of AXS was proposed in the last century, it has not been a particularly popular technique due to difficulties during experiment and data analysis. In this article, we report recent instrumental developments of dedicated AXS spectrometers at SPring-8 and review recent activities on fast phase-change materials, by combining AXS and large scale density functional theory (DFT)-based molecular dynamics (MD) simulations.

2. Anomalous x-ray scattering (AXS)[5,6]

The AXS technique utilizes the anomalous change of the atomic form factor of a specific element if the incident x-ray energy is near an absorption edge of the respective element. The complex atomic form factor of an element is given as

$$f(Q,E) = f_0(Q) + f'(E) + if''(E), \tag{2}$$

where $f_0(Q)$ is the usual energy-independent term, and $f'(E)$ and $f''(E)$ are the real and imaginary parts of the anomalous term, respectively. In general, $f(Q,E)$ is governed by the Q-dependent $f_0(Q)$ in a normal x-ray scattering process, and the anomalous term is negligible. When the incident x-ray energy approaches an absorption edge of a constituent element, however, $f'(E)$ has a large negative minimum and $f''(E)$ shows an abrupt jump near the corresponding absorption edge energy of each element. One can utilize the difference between two scattering spectra near an absorption edge of the ith element $\Delta_i I$, where one is typically measured at about 10 eV below, while the other at about 100 eV below the absorption edge (E_{near} and E_{far}, respectively). This differential intensity is expressed as

$$\alpha_i \Delta_i I(Q, E_{far}, E_{near}) = \Delta_i \left[\langle f^2 \rangle - \langle f \rangle^2 \right] + \Delta_i \left[\langle f \rangle^2 \right] \Delta_i S(Q), \tag{3}$$

where α_i is a normalization constant, and $\Delta_i[\ ]$ indicates the difference of values in the brackets at the energies of E_{far} and E_{near}, close to the absorption edge of the ith element. The $\Delta_i S(Q)$ functions are given by a linear combination of $S_{ij}(Q)$ as

$$\Delta_i S(Q) = \sum_{i=1}^{N} \sum_{j=1}^{N} w_{ij}(Q, E_{far}, E_{near}) S_{ij}(Q), \tag{4}$$

where the weighting factors are given by

$$w_{ij}(Q, E_{far}, E_{near}) = x_i x_j \frac{\Delta_i \left[f_i f_j \right]}{\Delta_i \left[\langle f \rangle^2 \right]}. \tag{5}$$

It should be noted that compared to $S(Q)$, $\Delta_i S(Q)$ highly enhances the contribution of the ith element related partial structure factors and suppresses other partials.

3. Instrumentation and typical AXS data

Two AXS spectrometers were developed at the single crystal structure analysis beamline BL02B1 and at the surface and interface structures beamline BL13XU [7] Figure 1 (a) shows a photograph of the AXS spectrometer developed at BL02B1. The standard setup of the 4-circle diffractometer with a Ge detector is used. The energy resolution of the spectrometer is $\Delta E = 500$eV at 12keV. The other AXS spectrometer built at beamline BL13XU, which is the dedicated high-resolution spectrometer employing a LiF analyzer crystal, is shown in Fig. 1(b). The spectrometer consists mainly of the standard six-circle diffractometer, slits, a beam stop, an analyzer crystal, and a NaI(Tl) scintillation detector.
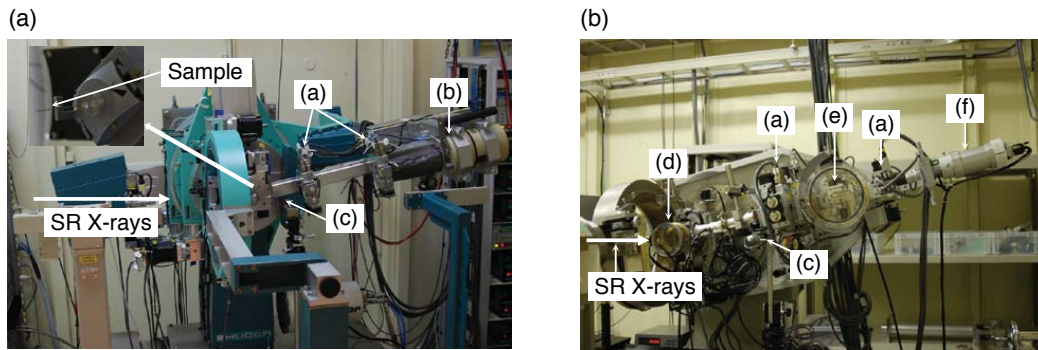
Figure 1. AXS spectrometer developed at (a) BL02B1 and at (b) BL13XU beamlines. (a) slits, (b) Ge detector, (c) beam stop, (d) vacuum chamber for sample, (e) LiF analyzer crystal, (f) NaI(Tl) scintillation detector

The ideal energy resolution ($\Delta E/E$) of an analyzer crystal is given by

$$\Delta E/E = \Delta\theta/\tan\theta_B, \tag{6}$$

where $\Delta\theta$ and θ_B are the rocking-curve width and the Bragg angle, respectively. By choosing an analyzer crystal with an adequate rocking-curve width, both a sufficient counting statistics and a sufficient energy resolution, to discriminate the contribution of fluorescence and of Compton scattering, can be achieved. In the case of 12 keV X-rays, LiF(200) reflection is appropriate choice for this purpose. In addition, it is notable that a LiF crystal is a low-cost product. A vacuum chamber is installed to suppress air scattering around the sample, which is very important to measure accurately when dealing with disordered materials. The vacuum chamber is useful for hygroscopic samples, too. High resolution in terms of energy is an important factor for precise AXS measurements, because fluorescence is induced by incident x-rays while measuring near the absorption edge. Figure 2(a) shows a typical rocking curve of the LiF(200) crystal for x-rays near 12 keV. The energy resolution is estimated to be 12 eV in FWHM, which allows us to discriminate the contributions from fluorescence and Compton scattering. Furthermore, the energy resolution of the LiF(200) crystal is approximately seven times better than that obtained by sagittal focusing of a cylindrical mosaic graphite crystal [6]. The total structure factor $S(Q)$ of amorphous $Ge_2Sb_2Te_5$ (a-GST) was measured at the Sb near edge. As it can be seen (Figure 2(b)), it is confirmed that raw scattering data can properly be normalized to give $S(Q)$, demonstrating that the high-energy resolution spectrometer succeeded in discriminating the contribution from fluorescence of Sb and from Compton scattering.

Figure 3(a) shows the differential structure factors $\Delta S(Q)$ for Nb of 25BaO-50Nb$_2$O$_5$-25P$_2$O$_5$ glass, together with the total structure factor $S(Q)$ obtained by high-energy x-ray diffraction (high-energy x-ray diffraction beamline BL04B2). Corresponding real space data are shown in Fig. 3(b). The contrast between normal x-ray diffraction data (black) and Nb K edge AXS data is excellent. Although the resolution in real space is different between two data sets, due to different Q_{max}, it is noted that the Ba-O correlation can be reasonably eliminated by AXS data. Furthermore, significant oscillations can be observed in 6 - 9 Å of AXS data, implying that niobium atoms exhibit specific ordering beyond the first coordination distance.
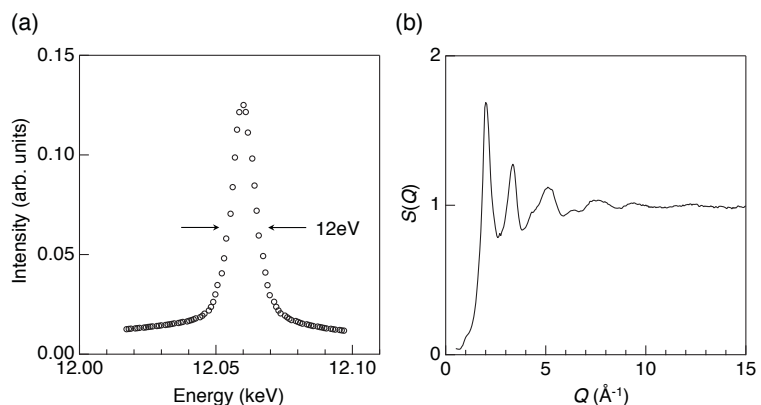

Figure 2. (a) Rocking curve of the LiF(200) crystal for x-rays near 12 keV and (b) total structure factor $S(Q)$ for a-GST measured at Sb near edge (E=30.462 keV).

4. Application to fast-phase change materials [8]

Although data storage on a DVD/Blu-ray is part of our digital world, the physical basis of the storage mechanism has not been fully understood in detail. Information is stored on a DVD in the form of microscopic bits in a thin layer of a polycrystalline alloy containing several elements. The bits can have a disordered, amorphous or an ordered, crystalline structure. The transition between the two phases lasts only tens of nanoseconds and can be triggered by a laser pulse [9]. The combination of AXS, HEXRD and Reverse Monte Carlo [10-12] / DFT-MD simulations has enabled the structures of both phases to be determined for the first time and allowed the development of a model that explains the rapid phase change and high durability. Figure 4(a) shows total scattering structure

Figure 3. (a) Differential structure factors $\Delta S(Q)$ for Nb of $25BaO-50Nb_2O_5-25P_2O_5$ glass together with the total structure factor $S(Q)$ obtained by high-energy x-ray diffraction measurement and (b) corresponding total correlation functions. The $S(Q)$ and $T(r)$ of HEXRD are displaced upward by 3 and 5, respectively, for clarity. Solid curves and dashed curve of $T(r)$ are obtained by Fourier transformation with Q_{max}=9.9 Å^{-1} and 25 Å^{-1}, respectively.

factors, $S(Q)$, for crystalline (c-) GST and a-GST. The diffraction pattern of c-GST exhibits sharp Bragg peaks and a diffuse scattering pattern, while only the latter appears for a-GST. It is demonstrated that $S(Q)$ of the RMC model (solid line) agrees well with experimental data (open circles). Differential structure factors, $\Delta S(Q)$, for Sb and Te, obtained from AXS measurements performed at BL02B1 using a germanium detector are shown in Fig. 4(b). As it can be seen in the figure, there are substantial differences between Sb- and Te-related data at $Q < 6$ Å^{-1}, demonstrating that AXS measurements can distinguish Sb (atomic number is 51) related correlation and Te (atomic number is 52) related correlation beyond the nearest neighbor distance.

Coordination numbers in a-GST are calculated up to 3.2 Å based on the RMC/DFT-MD model. In c-GST, both Ge and Sb are sixfold coordinated while the total coordination number of Te is 4.8, due to a vacancy on the Ge/Sb mixing site. These results are in line with the average structure of rocksalt, suggesting that disorder in the crystalline phase does not have any influence on average coordination

numbers. Baker et al. reported on the basis of EXAFS measurements [13] that both Ge and Sb obey the so-called '8-N rule' and that Te is overcoordinated in a-GST. Akola et al. reported overcoordinated Sb and Te on the basis of atomic configurations obtained by RMC/DFT-MD simulation using HEXRD data only [14]. In our new RMC model, refined by employing AXS data, total coordination numbers for Ge, Sb, and Te are 3.83, 3.06, and 2.45, respectively. Antimony has a lower coordination number than in the previous RMC/DFT-MD model (N_{Sb}=3.31 in ref. 14). As a result, now both Ge and Sb obey the '8-N rule' and only Te is overcoordinated. These results agree well with results of EXAFS measurements [13] and with that in
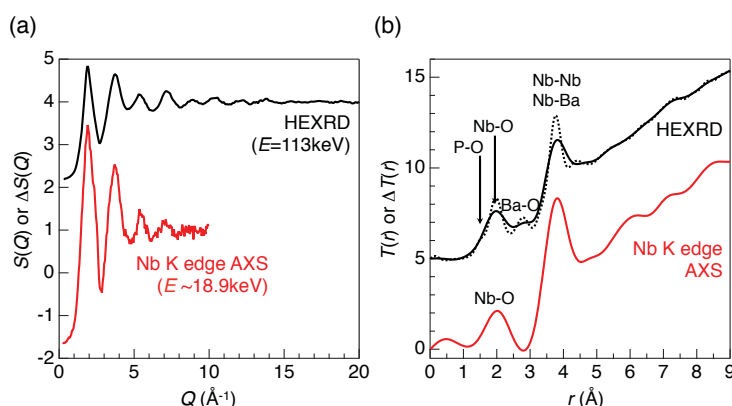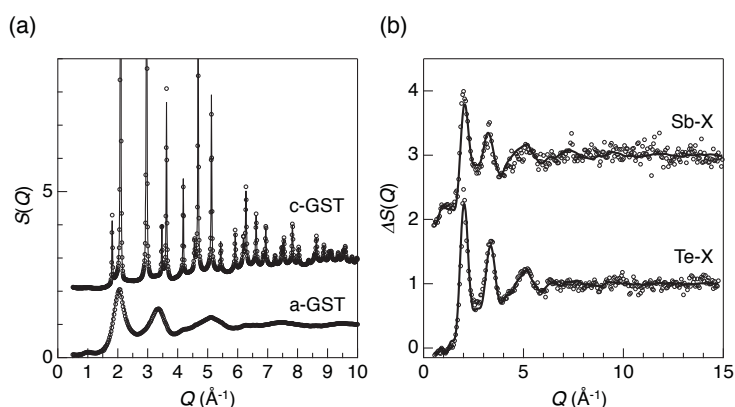
Figure 4. Comparison between the experimental structure factors (open circle) and results of RMC modelling (solid line). (a) Total scattering data for c-GST and a-GST obtained by HEXRD measurements. (b) $\Delta S(Q)$ for a-GST obtained by AXS measurements at Sb and Te K absorption edges. The $S(Q)$ of c-GST and the $\Delta S(Q)$ for Sb are displaced upward by 2 for clarity.

Olson et al.'s argument, in which they mentioned the possibility of overcoordinated Te if there are no homopolar (Ge-Ge, Sb-Sb, Te-Te) bonds in a-GST [15].

For obtaining statistical structural features beyond the nearest coordination distance, ring statistics were calculated using a shortest path analysis [16]. As can be seen in Fig. 5(a), fourfold and sixfold rings consisting of '–Ge(Sb)–Te–' units are dominant in c-GST. The existence of sixfold rings is due to the 20% vacancies on Ge/Sb mixing sites. As discussed in ref. 14, small '–Ge(Sb)–Te–' rings such as fourfold, fivefold, and sixfold rings are dominant in a-GST. The numbers of rings consisting of '–Ge–Te–' units and of '–Sb–Te–' units in a-GST are shown in Fig. 5(b). Our 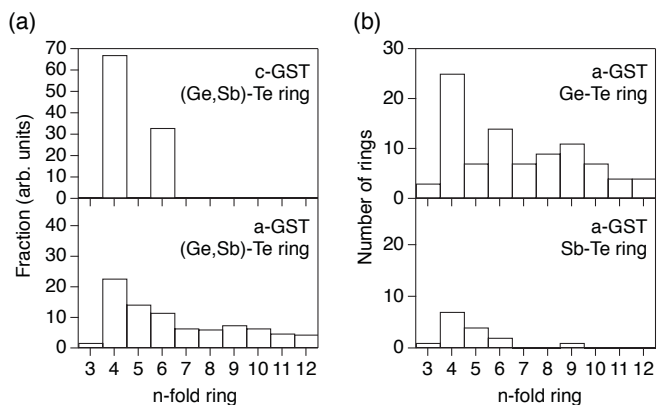new RMC model obtained by the introduction of AXS data suggests that large fractions of fourfold and sixfold rings are mainly

'–Ge(Sb)–Te–' rings. (b) Numbers of '–Ge–Te– rings' and '–Sb–Te– rings' in a-GST.

formed by Ge-Te bonds. Therefore it is suggested that the core network constructed by Ge-Te covalent bonds in a-GST is similar to that in c-GST, and that this core network plays an important role in stabilizing the amorphous phase at room temperature for long time.

To understand the atomic ordering by Ge-Te and Sb-Te bonds in detail, connectivities of atoms were calculated, with varying the maximum distance within which atomic pairs were considered to be connected. As can be seen in Fig. 6(a), about 60% of Ge-Te bonds up to 3.2 Å form a continuous core network whereas Sb-Te bonds up to 3.2 Å do not form such a network. This distance corresponds to the covalent bond distance determined by DFT-MD simulation [17] and both Ge and Sb satisfy the '8-N rule' at 3.2 Å in our new RMC model (N_{Ge}=3.83 and N_{Sb}=3.06). Atomic configurations of Ge-Te and Sb-Te with bonds considered up to 3.2 Å are shown in Fig. 6(b). It can be clearly distinguished that Ge-Te bonds form a core network, which stabilizes the amorphous phase, whereas Sb-Te bonds

do not. Furthermore it is evident that Ge-Te bonds form large fractions of fourfold (highlighted by blue) and sixfold (highlighted by light blue) rings. On the other hand, about 70 % of the Sb-Te pairs form a pseudo network, as can be seen in Figs. 6(a) and 6(c), when bonds are considered up to 3.5 Å (this way, the coordination numbers of Te around Ge (N_{Ge-Te}) and Sb (N_{Sb-Te}) are 4.08 and 3.08, respectively). In other words, the pseudo Sb-Te network becomes visible when we extend the correlation distance up to 3.5 Å, while such a feature cannot be observed for Ge-Te connectivities. On the basis of structural features in a-GST displayed above, we discuss the role of each elements in the phase-change process. As highlighted by red in Fig. 6(b), Ge-Te bonds significantly contribute to the network containing by fourfold rings. Therefore Ge and Te can be recognized as network forming elements that stabilize the amorphous phase at room temperature for
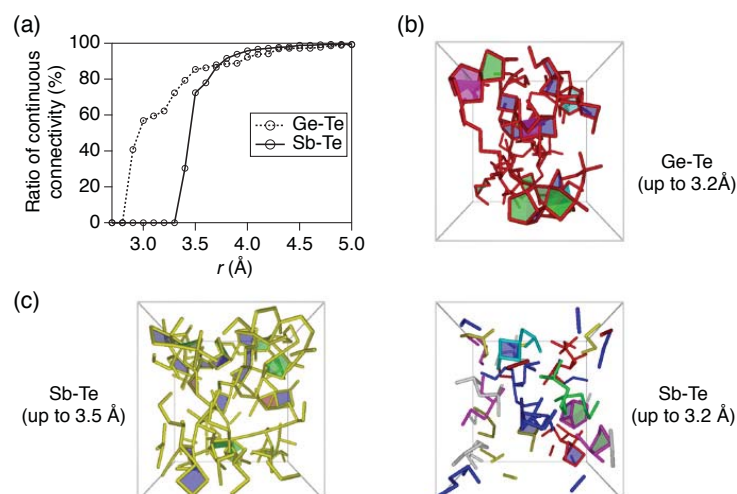

Figure 6. Atomic configuration and connectivity of Ge-Te and Sb-Te in a-GST obtained by the RMC model. (a) Connectivity of Ge-Te and Sb-Te with different r_{max}. (b) Atomic configuration of Ge-Te and Sb-Te (connectivity of Ge-Te and Sb-Te considered up to 3.2 Å). (c) Atomic configuration of Sb-Te (connectivity of Sb-Te considered up to 3.5 Å). The theeefold, fourfold, fivefold, and sixfold rings are highlighted by red, blue, green, and light blue, respectively.

long time. The core Ge-Te network may remain in the crystalline phase, which feature explains rapid crystallization. As highlighted by yellow in Fig. 6(c), Sb-Te correlations beyond the nearest coordination distance form a pseudo Sb-Te network. This unusual atomic ordering in terms of Sb-Te correlations can be ascribed to the combination of two positively charged atoms (Ge, -0.22 electrons; Sb, 0.32 electrons; Te, 0.22 electrons [19]) and allows the amorphous phase to form critical nuclei via forming Sb-Te bonds by small atomic displacements of antimony and tellurium atoms. Thus our finding can reasonably explain the reason why the crystallization of amorphous GeTe (a-GT) is very fast in PC-RAM [18] and the reason why the crystallization of a-GST is faster than that of a-GT in DVD [19].

5. Conclusion
We have succeeded in developing AXS spectrometers at SPring-8. The high-energy resolution spectrometer provides us with sufficient energy resolution to discriminate the contribution of fluorescence and of Compton scattering. In addition, the photon flux of x-rays from a SPring-8 undulator is high enough to perform AXS measurement of disordered materials. Therefore a combination of HEXRD and AXS is a powerful tool to understand the atomic arrangement of complicated functional disordered materials. Furthermore a combination of advanced synchrotron radiation measurements and massive super computing is essential to uncover the relationship between the structure of functional disordered materials at atomic/ electronic level [20] and their function.

References
[1] Poulsen H F, Neuefeind J, Neumann H-B, Schneider J R and Zeidler M D 1995 *J. Non-Cryst. Solids* **188** 63
[2] Kohara S, Itou M, Suzuya K, Inamura Y, Sakurai Y, Ohishi Y and Takata M 2007 *J. Phys.: Condens. Matter* **19** 506101
[3] Benmore C J, 2012 *ISRN Mater. Sci.* doi:10.5402/2012/852905
[4] Salmon P S 2002 *Nature Mater.* **1** 87
[5] Waseda Y 2002 *Anomalous x-ray scattering for materials characterization* (Heidelberg, Springer)
[6] Hosokawa S, Wang Y, Bérar J-F, Greif J, Pilgrim W-C and Murase K 2002 *Z. Phys. Chem.* **216** 1219
[7] Sakata O, Furukawa Y, Goto S, Mochizuki T, Uruga T, Takeshita K, Ohashi H, Ohata T, Matsushita T, Takahashi S, Tajiri H, Ishikawa T, Nakamura N, Ito M, Sumitani K, Takahashi T, Shimura T, Saito A and Takahasi M 2003 *Surf. Rev. Lett.* **10** 543
[8] Ohara K, Temleitner L, Sugimoto K, Kohara S, Matsunaga T, Pusztai L, Itou M, Ohsumi H, Kojima R, Yamada N, Usuki T, Fujiwara A and Takata M 2012 *Adv. Func. Mater.* **22** 2251
[9] Wuttig M and Yamada N 2007 *Nature Mater.* **6** 824
[10] McGreevy R L, Pusztai L 1988 *Molec. Simul.* **1** 359
[11] Mellergård A, McGreevy R L 1999 *Acta. Cryst.* **55** 783
[12] Gereben O, Jóvári P, Temleitner L and Pusztai L 2007 *J. Optoelectron. Adv. Mater.* **9** 3021
[13] Baker D A, Paesler M A, Lucovsky G, Agarwal S C and Taylor P C 2006 *Phys. Rev. Lett.* **96** 255501
[14] Akola J, Jones R O, Kohara S, Kimura S, Kobayashi K, Takata M, Matsunaga T, Kojima R and Yamada N. 2009 *Phys. Rev. B* **80** 020201
[15] Olson J K, Li H and Taylor P C 2005 *J. Ovonic Res.* **1** 1
[16] Guttman L 1990 *J. Non-Cryst. Solids* **116** 145
[17] Akola J and Jones R O 2008 *J. Phys.: Condens. Matter* **20** 465103
[18] Bruns G, Merkelbach P, Schlockermann C, Salinga M, Wuttig M, Happ T D, Philipp J B and Kund M, 2009 *Appl. Phys. Lett.* **95** 043108
[19] Coombs J H, Jongenelis A P J M, Es-Spiekman W v and Jacobs B A J 1995 *J. Appl. Phys.* **78** 4918
[20] Akola J, Kohara S, Ohara K, Fujiwara A, Watanabe Y, Masuno A, Usuki T, Kubo T, Nakahira A, Nitta K, Uruga T, Weber J K R and Benmore C J 2013 *Proc. Natl. Acad. Sci. USA* **110** 10129